Article

Irradiation Hardening Behavior of He-Irradiated V–Cr–Ti Alloys with Low Ti Addition

Ken-ichi Fukumoto [1],*, Yoshiki Kitamura [1], Shuichiro Miura [1], Kouji Fujita [1], Ryoya Ishigami [2] and Takuya Nagasaka [3]

[1] Research Institute of Nuclear Engineering, University of Fukui, Tsuruga, Fukui 914-0055, Japan; ha170518@u-fukui.ac.jp (Y.K.); jn190083@u-fukui.ac.jp (S.M.); jn180098@u-fukui.ac.jp (K.F.)
[2] The Wakasa Wan Energy Research Center, Tsuruga, Fukui 914-0192, Japan; rishigami@werc.or.jp
[3] National Institute of Fusion Science, Toki, Gifu 509-5292, Japan; nagasaka@nifs.ac.jp
* Correspondence: fukumoto@u-fukui.ac.jp

Abstract: A set of V–(4–8)Cr–(0–4)Ti alloys was fabricated to survey an optimum composition to reduce the radioactivity of V–Cr–Ti alloys. These alloys were subjected to nano-indenter tests before and after 2-MeV He-ion irradiation at 500 °C and 700 °C with 0.5 dpa at peak damage to investigate the effect of Cr and Ti addition and gas impurities for irradiation hardening behavior in V–Cr–Ti alloys. Cr and Ti addition to V–Cr–Ti alloys for solid–solution hardening remains small in the unirradiated V–(4–8)Cr–(0–4)Ti alloys. Irradiation hardening occurred for all V–Cr–Ti alloys. The V–4Cr–1Ti alloy shows the highest irradiation hardening among all V–Cr–Ti alloys and the gas impurity was enhanced to increase the irradiation hardening. These results may arise from the formation of Ti(CON) precipitate that was produced by He-ion irradiation. Irradiation hardening of V–Cr–1Ti did not depend significantly on Cr addition. Consequently, for irradiation hardening and void-swelling suppression, the optimum composition of V–Cr–Ti alloys for structural materials of fusion reactor engineering is proposed to be a highly purified V–(6–8)Cr–2Ti alloy.

Keywords: vanadium alloy; ion irradiation; irradiation hardening; radiation damage

1. Introduction

Vanadium alloys are attractive blanket structural materials in fusion power systems because of their low induced activation characteristics, high-temperature strength, good compatibility with a liquid lithium environment and high thermal stress [1–3]. Critical issues of vanadium alloys, such as corrosion and oxidation have been resolved by Cr and Ti addition to the vanadium matrix, and recent efforts have focused on developing the V–4Cr–4Ti alloy as a candidate alloy for Li-blanket systems in fusion reactors [4,5]. The susceptibility of V–4Cr–4Ti alloys to low-temperature embrittlement during neutron irradiation may limit their application in low-temperature (<400 °C) regimes [6]. To improve this drawback, highly purified V–4Cr–4Ti alloys, such as NIFS-HEAT-1 and -2, have been developed by the National Institute for Fusion Science (NIFS) [7–10]. The NIFS-HEAT-2 has shown significantly lower radioactivity for full remote recycle over 25 years of cooling after being used in the first wall of a fusion commercial reactor. A reduction in the cooling period provides economical and safety benefits to reduce the amount of radiation waste material [11].

Nagasaka suggested that the cooling period of V–Cr–Ti alloy for full remote recycling can be reduced within 10 years by reducing the Ti addition from a V–4Cr–4Ti alloy [12]. The reduction in Ti addition reduces the cooling time and results in swelling and a loss of mechanical strength under neutron irradiation.

To optimize the Ti and Cr addition to V–Cr–Ti alloys to balance the irradiation hardening and swelling behavior, a set of V–Cr–Ti alloys with a lower Ti content and higher Cr content was produced from V–4Cr–4Ti alloys. In this study, nano-indenter tests were

performed to investigate irradiation hardening in a new set of V–Cr–Ti alloys after He-ion irradiation to survey the optimum composition to compensate between radioactivity reduction and irradiation hardening behavior in V–Cr–Ti alloys.

2. Experimental Procedure

In total, 15 types of V–(4–8)Cr–(0–4)Ti ternary alloys were fabricated by arc melting. Table 1 shows the chemical composition of the V–Cr–Ti alloys that were used in this study. Two impurity levels of each alloy were prepared to investigate the effect of interstitial impurity for irradiation hardening during He-ion irradiation. The highly purified alloy was marked as "(h)". The V–Cr–Ti alloys from conventional fabrication contain ~500 ppm of C+N–O interstitial gas impurity. In contrast, highly purified V–Cr–Ti alloys, which are marked as "(h)", contain approximately half the interstitial gas impurity in conventional alloys by using highly purified vanadium ingots in fabrication [11]. Thin specimen plates of 10 mm × 2 mm × 0.2 mm were cut out and annealed for 2 h at 1000 °C in a vacuum ($\sim 2 \times 10^{-4}$ Pa). The samples were irradiated with 2-MeV ^{4}He ions using a tandem accelerator at the Wakasa Wan Energy Research Center. Sectional shapes of the ^{4}He^{2+} beams existed in a 9-mm-diameter circle or ellipse with a major axis of 10 mm and a minor axis of 6 mm. These beams were scanned to irradiate the samples uniformly. The horizontal and vertical widths of the scanned beams were 13 mm × 13 mm for the former beam and 13 mm × 17 mm for the latter beam. Time-averaged current densities were 0.4 µA/cm^2 and 0.9 µA/cm^2, respectively. During the irradiation, the sample stage was heated on a Mo holder with a ceramic heater. The temperature was maintained within ± 5 °C during ion irradiation. Specimens were irradiated at 500 °C and 700 °C up to doses of 0.5 dpa at a peak position and 3.4 µm depth.

Table 1. Chemical composition of V–Cr–Ti alloys. Marks (h) indicate the type of highly purified alloy from the original alloy.

Composition (wt.%)	Cr	Ti	C	N	O	Mo	Al	Si
V-4Cr	3.80	0.002	0.004	0.005	0.036	(<0.001)	0.005	(0.02)
V-4Cr (h)	3.90	0.002	0.009	0.003	0.018	(<0.001)	0.011	(0.02)
V-4Cr-0.1Ti	3.88	0.09	0.005	0.005	0.038	(<0.001)	0.012	(0.02)
V-4Cr-0.1Ti (h)	3.90	0.09	0.007	0.003	0.017	(<0.001)	0.011	(0.02)
V-4Cr-1Ti	3.86	0.96	0.005	0.006	0.035	<0.001	0.006	0.016
V-4Cr-1Ti (h)	4.02	0.96	0.008	0.004	0.016	(<0.001)	0.009	(0.02)
V-4Cr-2Ti	3.94	1.93	0.005	0.005	0.037	(<0.001)	0.005	(0.02)
V-4Cr-2Ti (h)	3.89	1.92	0.008	0.003	0.015	(<0.001)	0.006	(0.02)
V-4Cr-3Ti (h)	3.92	2.99	0.009	0.003	0.016	(<0.001)	0.007	(0.02)
V-4Cr-4Ti	3.93	3.91	0.006	0.006	0.036	<0.001	0.009	0.016
V-4Cr-4Ti (h)	4.11	3.89	0.008	0.003	0.018	(<0.001)	0.018	(0.02)
V-6Cr-1Ti	5.97	0.96	0.006	0.006	0.036	<0.001	0.006	0.016
V-6Cr-1Ti (h)	5.95	0.95	0.010	0.003	0.015	(<0.001)	0.016	(0.02)
V-8Cr-1Ti	7.89	0.99	0.006	0.006	0.038	<0.001	0.008	0.016
V-8Cr-1Ti (h)	7.83	1.00	0.008	0.003	0.015	(<0.001)	0.016	(0.02)

Figure 1 shows the damage profile and He ion range in vanadium as calculated by using the SRIM-code (the stopping and range of ions in matter). After He ion irradiation, a nano-indentation test was examined at room temperature by using a Elionix ENT-1100a (Elionix Inc., Tokyo, Japan) nano-indenter with a Berkovich diamond indenter tip and a direction of indentation parallel to the ion beam axis, which is normal to the irradiated surface. The nano-indenter test was carried out with an indentation depth of 500 nm. The indentation depth was determined from the effective depth where the plastic and elastically deformed area was expanded during the nano-indenter test that corresponds to five times the length of the nano-indenter depth. To avoid uncertainty about the specimen surface condition, a scanning electron microscopy (SEM) observation with electron backscattered diffraction measurement was carried out on the indentation surface after the indentation test to ascertain that the indentation test was not on/near grain boundary on the specimen

surface. For each sample, 12 tests were conducted, and 10 of the measured data points were included in the analysis, rejecting the maximum and minimum measured values. In this study He ions were used as the projectile because the penetration depth is sufficient to assess mechanical properties as irradiation hardening through nano-indentation hardness measurements [13]; it should be noted that the first wall and divertor of a fusion reactor are expected to be subject to high fluxes of moderate to low-energy helium ions created as fusion reaction products and as a result He bubbles may form around the He ion penetration range which was 3.6 μm in this study.
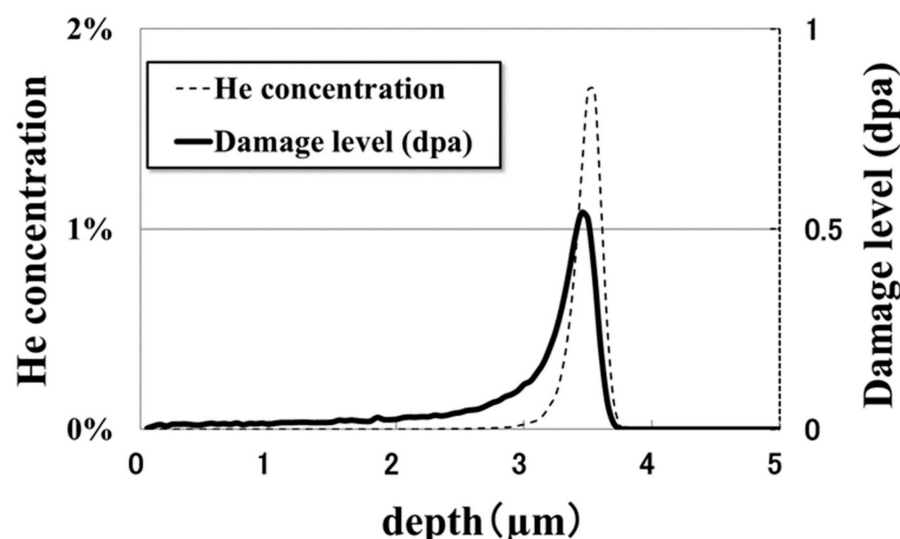

Figure 1. Calculation results of ion range profile of implanted He ion and vacancy concentration profile in V by 2-MeV He$^+$ ion irradiation.

3. Results

Figure 2 shows the results from the nano-indenter test for unirradiated V–4Cr–xTi alloys and He-irradiated V–4Cr–xTi alloys at 500 °C. In the unirradiated V–4Cr–xTi alloys, the effects of Ti addition and interstitial gas impurity on the nano-indentation hardness were not apparent. The hardness of the V–4Cr–xTi and V–4Cr–xTi(h) alloys did not change at ~1800 N/mm^2. The He-irradiated V–4Cr–xTi alloys showed a large irradiation hardening. V–4Cr–1Ti showed the largest irradiation hardening of the alloys and the hardness reached 5100 N/mm^2, which was approximately 2.8 times larger than the hardness of unirradiated V-4Cr-1Ti alloys. For the V–4Cr–xTi with 2% to 4% Ti addition, the irradiation hardening decreased and did not change as much with increasing Ti addition. Therefore 1% Ti addition is most effective to produce irradiation hardening in V–4Cr–xTi (x = 0 to 4). From 0.1% to 1%Ti addition in V–4Cr–xTi alloys, the alloys that contained more interstitial gas impurity showed a larger increase in irradiation hardening. V–4Cr–xTi alloys that contained more than 2% Ti addition did not change the irradiation hardening increase even though the amount of gas interstitial impurity increased. This result suggests that the interstitial gas impurity does not contribute to irradiation hardening in V–4Cr–xTi alloys with more than 2% Ti addition.

Figure 3 shows the irradiation hardening increase of V–4Cr–xTi alloys with the conventional impurity level irradiated at 500 °C and 700 °C. The He-irradiated V–4Cr–xTi alloys at 700 °C showed irradiation hardening but the amount of irradiation hardening increase at 700 °C was smaller than that at 500 °C. This result indicates that damaged microstructures that formed at 700 °C irradiation may be coarser than those formed at 500 °C irradiation, and irradiation hardening at 700 °C irradiation is smaller than that at 500 °C irradiation. These microstructural features depending on irradiation temperature and damage level have been reported elsewhere [5,14,15].
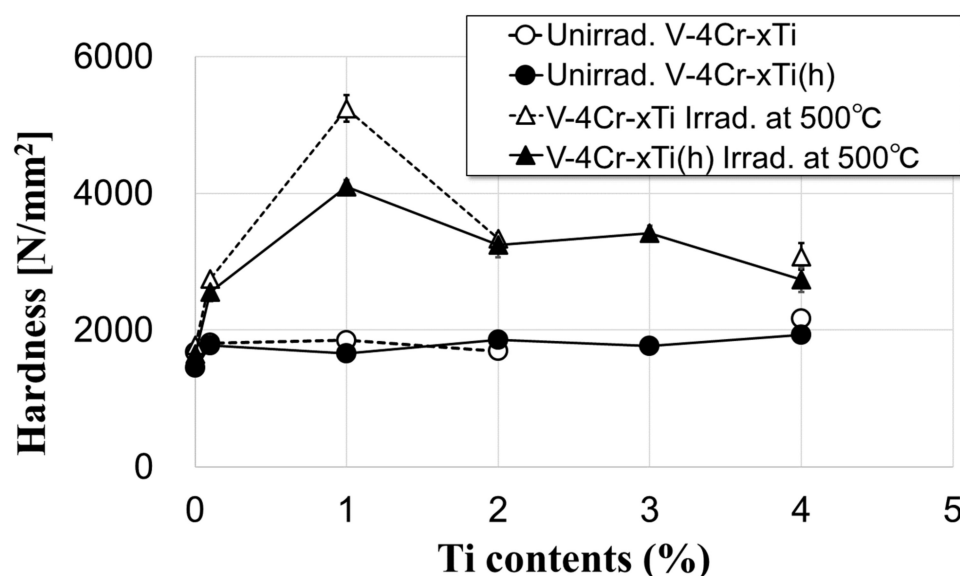
Figure 2. Ti content dependence of nano-indentation hardening for unirradiated V–4Cr–xTi alloys and He-irradiated V–4Cr–xTi alloys at 500 °C.
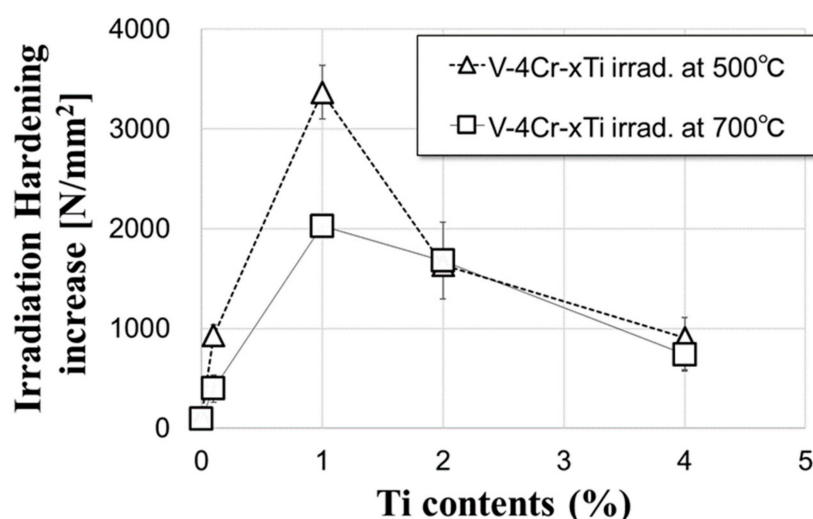

Figure 3. Irradiation hardening increase of V–4Cr–xTi alloys with conventional impurity level irradiated at 500 °C and 700 °C as a function of Ti content.

Figure 4 shows the nano-indenter test results for unirradiated and He-irradiated V–yCr–1Ti alloys with a conventional impurity level irradiated at 500 °C and 700 °C. In the unirradiated V–yCr–1Ti alloys, the nano-indentation hardness of the V–yCr–1Ti alloys increased slightly with an increase in Cr addition, which was caused by solution hardening because of Cr addition in V–Cr–Ti alloys. The interstitial gas impurity in the V–yCr–1Ti alloys did not affect the hardening behavior much. Irradiation hardening of He-irradiated V–yCr–1Ti was apparent in all alloys. Significant irradiation hardening occurred among all alloys, but the irradiation hardening decreased with an increase in Cr addition. The significant reduction in irradiation hardening in the V–8Cr–1Ti alloys was apparent. The effect of interstitial gas impurity on the irradiation-hardening behavior of V–yCr–1Ti showed that the conventional fabricated alloys had a larger irradiation hardening increase than the highly purified alloys. The irradiation hardening at 500 °C irradiation was larger than that at 700 °C irradiation in all V–yCr–1Ti alloys. At 500 °C irradiation, the irradiation hardening decreased with an increase in Cr addition. The irradiation hardening of the V–yCr–1Ti alloys that were irradiated at 700 °C increased with an increase in Cr addition.

From the result of heat treatment of V-4Cr-4Ti alloys at high temperatures, it has been reported that fine precipitate forms above 700 °C of annealing temperature [16]. Hence, it is concluded that the hardness increase at 500 °C in this study is not solely caused by the precipitation induced by the irradiation temperature at least.
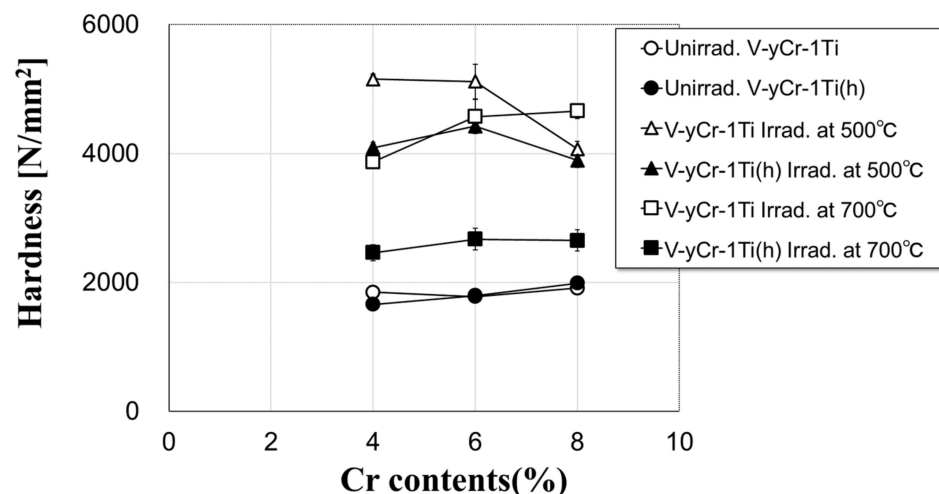

Figure 4. Cr content dependence of nano-indentation hardening for unirradiated V–yCr–1Ti alloys and He-irradiated V–yCr–1Ti alloys at 500 °C and 700 °C.

4. Discussion

Previous work on the thermal creep deformation of V–Ti alloy indicated that 3% Ti addition to V resulted in the lowest activation energy for creep strain behavior in the V–xTi alloys (x = 0% to 20%) [17–19]. The low activation energy of creep deformation reduces the creep strain rate at a given temperature in the material and leads to a high creep strength. The creep strength is strengthened by Ti addition to V in the V–Ti system alloy from the increase in yield and tensile strengths because of a solid–solution hardening mechanism and/or a dispersed particle-strengthening mechanism. The main reason why the V–3Ti alloy exhibits the strongest creep strength in the V–Ti system alloy (0% to 20% Ti addition) cannot be explained by the solid–solution hardening mechanism because solid–solution hardening due to Cr and Ti addition to V–Cr–Ti alloys was not apparent in this work as determined from the nano-indentation test of unirradiated V–Cr–Ti alloys as shown in Figure 2. In the thermal creep deformation in V–Ti alloy at an elevated temperature, the formation of a dislocation-network as well as formation of a titanium-oxycarbonitride precipitate, Ti(CON) have been observed as thermal vacancy migration and dislocation slip motion. Figure 5 provides an example of precipitate formation in V–4Cr–4Ti alloys in creep deformation at 600 °C with a stress of 200 MPa for 2800 h in a liquid Na environment [20]. Small precipitates formed near the grain boundary or large bulk precipitates and the precipitate was Ti(CON) titanium-oxycarbonitride precipitate on a habit pane of {100}. The nature of the Ti(CON) precipitate has been reported by Impagnatiello [21–23]. In the thermal creep test, it is likely that Ti(CON) precipitates are formed along with defect sinks such as grain boundaries and bulk precipitates where the thermal vacancy is absorbed preferentially. It is expected that the Ti(CON) precipitate is more likely to form in an environment where that migration of Ti is enhanced due to vacancy flux to sinks such as grain boundaries through the Kirkendall effect for a long period and the nucleation of Ti(CON) precipitate occurs around sinks such as grain boundaries and large bulk precipitates due to the thermal heat treatment. Since He irradiation at high temperature also provides a large defect flux of not only excess vacancies but also displaced Ti atoms produced by He ion bombardment in the matrix, this kind of irradiation may lead to the formation of Ti(CON) precipitates in the matrix. Previous transmission electron microscopy (TEM) work for the microstructural observation of neutron- and ion-irradiated V–Cr–Ti and V–Ti alloys reported that Ti(CON) precipitate formation occurred above 350 °C with more

than 0.1 dpa of damage level [24–28]. It is deduced that the significant irradiation hardening in V–Cr–Ti alloys in this work was caused by irradiation-induced Ti(CON) precipitation during 500 °C and 700°C irradiation, even though microstructural observation by TEM work remained unexamined in this work. The high density of small Ti(CON) precipitate formed in V–4Cr–1Ti alloys and V–4Cr–1Ti shows the highest obstacle resistance against dislocation slip based on the Orowan equation termed as dispersed barrier hardening in [29];

$$\Delta\sigma\_y = M\alpha\mu b\sqrt{ND} \tag{1}$$

where M is the Taylor factor (3.06 for fcc polycrystals), μ the shear modulus of the matrix, b the magnitude of the Burgers vector of the moving dislocation, and $\Delta\sigma_y$ represents the increment in yield strength because of the obstacles of size D, number density, N and barrier strength α. It is assumed that the density of small precipitate in V–4Cr–1Ti will be highest among all V-4Cr–xTi and shows a significant irradiation hardening based on the dispersed precipitate hardening produced by He-ion irradiation.
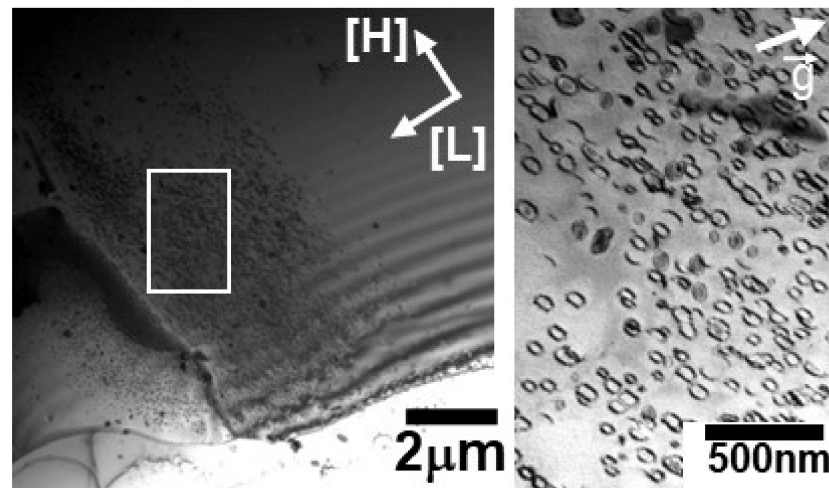

Figure 5. TEM micrographs of thermal-creep-deformed V–4Cr–4Ti alloy at 600 °C and 150 MPa for 2800 h. The left side of the low-magnification image shows that precipitates gathered along a grain boundary and the right side of the high magnification image shows that precipitates on {100} habit plane were formed. [L] and [H] indicate the direction of the longitudinal direction and horizontal direction of the creep tube, respectively. (after Fukumoto et al. [20]).

The nano-indentation test results from the V–Cr–Ti alloys show that the unirradiated V–6Cr–1Ti and V–8Cr–1Ti alloy hardness did not change much compared with that of the V–4Cr–1Ti alloys. Therefore, Cr addition may be ineffective for solid–solution hardening in V–Cr–Ti alloys. The He-irradiated V–yCr–1Ti alloy results show that the effect of Cr addition for irradiation hardening is independent of Cr addition in the V–(4–8)Cr–Ti alloys.

The effect of gas impurity level for irradiation hardening appears in irradiation hardening of V–4Cr–1Ti alloys irradiated at 500 °C and 700 °C, and the highly purified V–Cr–Ti alloys reduce the irradiation hardening as shown in Figures 2 and 4. This reduction of irradiation hardening in highly purified V–Cr–Ti alloys may be caused by the formation of Ti(CON) precipitates during He-ion irradiation. The nucleation and growth of Ti(CON) precipitate should be rate-limited to the concentration of gas impurities of C, N and O, and Ti atoms and the nucleation rate is proportional to the product $C_{imp} \cdot C_{Ti}$ of the gas impurity concentration C_{imp} and Ti concentration C_{Ti} from the kinetics of the point defect reaction [30], when the nuclei of Ti(CON) are assumed to be TiO- or TiC-type [31]. The reduction in gas impurities in the V–Cr–Ti alloy matrix is connected with the nucleation rate of Ti(CON) precipitate and a decrease of irradiation hardening in the V–Cr–Ti alloys.

Microstructural observation by TEM is required to clarify the correlation between irradiation hardening and microstructural evolution, and especially Ti(CON) formation in the future.

Because V–4Cr–1Ti alloys show significant irradiation hardening and more than 2% Ti addition to V–4Cr–xTi alloys results in a lower irradiation hardening than the V–4Cr–1Ti alloy, the optimum amount of Ti addition to candidate alloys for structural materials of fusion reactor application should be 2% to avoid surplus irradiation hardening at low-temperature irradiation. In terms of the swelling behavior of V–Cr–Ti alloys, 1% Ti addition to V–Cr–Ti and V–Fe–Ti alloys is enough to suppress void swelling from 400 to 600 °C with heavy damage levels to 30 dpa [32]. Hence, 2% Ti addition to V–Cr–Ti alloys helps to suppress void swelling at a high temperature with heavy damage. Consequently, from the viewpoints of the suppression of surplus irradiation hardening and void swelling, an optimum composition of V–Cr–Ti alloys for structural materials of fusion reactor engineering is proposed to be a highly purified V–(6–8)Cr–2Ti.

5. Conclusions

To survey an optimum composition to reduce the radioactivity in V–Cr–Ti alloys, 15 types of V–(4–8)Cr–(0–4)Ti alloys were fabricated. These alloys were subjected to 2-MeV He-ion irradiation using a tandem accelerator at the Wakasa Bay Energy Research Center. Specimens were irradiated at 500 °C and 700 °C up to doses of 0.5 dpa at peak positions in 3.6 μm depth. To investigate the effect of Cr and Ti addition and gas impurities for irradiation hardening behavior in the V–Cr–Ti alloys, nano-indentation tests were examined at room temperature. Cr and Ti addition to V–Cr–Ti alloys for solid–solution hardening is low in the unirradiated V–(4–8)Cr–(0–4)Ti alloys. Irradiation hardening could be observed among all V–Cr–Ti alloys irradiated at 500 °C and 700 °C. The V–4Cr–1Ti alloy irradiated at 500 °C shows the highest irradiation hardening among all V–Cr–Ti alloys and the irradiation hardening was 2.8 times larger than the hardness of unirradiated V–4Cr–1Ti alloy. The gas impurity increased the irradiation hardening in V–4Cr–xTi alloys. The Cr addition dependence on irradiation hardening to V–yCr–1Ti was not remarkable. The effect of interstitial gas impurity for irradiation hardening of V–yCr–Ti showed that the conventional fabricated alloys had a larger irradiation hardening increase than the highly purified alloys. The significant irradiation hardening in V–4Cr–1Ti is caused by the formation of Ti(CON) precipitate from He-ion irradiation. Because the thermal creep strength of the V–3Ti is highest among all V–Ti system alloys and small precipitates formed in thermal-creep deformed V–4Cr–4Ti alloys in previous studies, the formation of Ti(CON) precipitate results from hardening during irradiation. Consequently, to suppress irradiation hardening and void swelling, the optimum composition of V–Cr–Ti alloys for structural materials of fusion reactor engineering is proposed to be a highly purified V–(6–8)Cr–2Ti alloy.

References

1. Matsui, H.; Fukumoto, K.; Smith, D.; Chung, H.M.; Van Witzenburg, W.; Votinov, S. Status of vanadium alloys for fusion reactors. *J. Nucl. Mater.* **1996**, *233*, 92–99. [CrossRef]

2. Kurtz, R.J.; Abe, K.; Chernov, V.M.; Hoelzer, D.T.; Matsui, H.; Muroga, T.; Odette, G.R. Vanadium alloys for fusion blanket ap-plications. *J. Nucl. Mater* **2004**, *329–333*, 47–55. [CrossRef]

3. Muroga, T.; Chen, J.; Chernov, V.; Kurtz, R.; Le Flem, M. Present status of vanadium alloys for fusion applications. *J. Nucl. Mater.* **2014**, *455*, 263–268. [CrossRef]

4. Smith, D.L.; Chung, H.M.; Loomis, B.A.; Tsai, H.-C. Reference vanadium alloy V-4Cr-4Ti for fusion application. *J. Nucl. Mater.* **1996**, *233*, 356–363. [CrossRef]

5. Chung, H.M.; Loomis, B.A.; Smith, D.L. Properties of V-4Cr-4Ti for application as fusion reactor structural components. *Fusion Eng. Des.* **1995**, *29*, 455–464.

6. Zinkle, S.J.; Matsui, H.; Smith, D.; Rowcliffe, A.; Van Osch, E.; Abe, K.; Kazakov, V. Research and development on vanadium alloys for fusion applications. *J. Nucl. Mater.* **1998**, *258*, 205–214. [CrossRef]

7. Nagasaka, T.; Muroga, T.; Imamura, M.; Tomiyama, S.; Sakata, M. Fabrication of high-purity V-4Cr-4Ti low activation alloy products. *Fusion Technol.* **2001**, *39*, 659–663. [CrossRef]

8. Muroga, T.; Nagasaka, T.; Abe, K.; Chernov, V.M.; Matsui, H.; Smith, D.L.; Xu, Z.-Y.; Zinkle, S.J. Vanadium alloys—Overview and recent results. *J. Nucl. Mater.* **2002**, *307*, 547–554. [CrossRef]

9. Nagasaka, T.; Muroga, T.; Yican, W.; Zengyu, X.; Imamura, M. Low activation characteristics of several heats of V-4Cr-4Ti ingots. *J. Plasma Fusion Res. Ser.* **2002**, *5*, 545–550.

10. Muroga, T. Vanadium alloys for fusion blanket application. *Mater. Trans.* **2005**, *46*, 405–411. [CrossRef]

11. Tanaka, T.; Nagasaka, T.; Muroga, T.; Yamazaki, M.; Toyama, T. Activation analysis for the reference low-activation vanadium alloy NIFS-HEAT-2. *Nucl. Mater. Eng.* **2020**, *25*, 100782. [CrossRef]

12. Nagasaka, T. Unpublished Work in Grant-in-Aid for Scientific Research (A) 20H00144, 2020, Japan. Available online: https://kaken.nii.ac.jp/grant/KAKENHI-PROJECT-20H00144/ (accessed on 31 December 2020).

13. Saleh, M.; Xu, A.; Hurt, C.; Ionescu, M.; Daniels, J.E.; Munroe, P.; Edwards, L.; Bhattacharyya, D. Oblique cross-section nanoindentation for determining the hardness change in ion-irradiated steel. *Int. J. Plast.* **2019**, *112*, 242–256. [CrossRef]

14. Fukumoto, K.; Matsui, H.; Chung, H.; Gazda, J.; Smith, D. Helium behavior in vanadium-based alloys irradiated in the dynamic helium charging experiments. *Sci. Rep. Res. Inst. Tohoku Univ. A Phys. Chem. Met.* **1997**, *45*, 149–155.

15. Fukumoto, K.; Onitsuka, T.; Narui, M. Dose dependence of irradiation hardening of neutron irradiated vanadium alloys by using temperature control rig in JMTR. *Nucl. Mater. Energy* **2016**, *9*, 441–446. [CrossRef]

16. Heo, N.J.; Nagasaka, T.; Muroga, T. Effect of impurity levels on precipitation behavior in the low-activation V–4Cr–4Ti alloys. *J. Nucl. Mater.* **2002**, *307–311*, 620–624. [CrossRef]

17. Yaggee, F.L.; Gilbert, E.R.; Styles, J.W. Thermal expansivities, thermal conductivities, and densities of vanadium, titanium, chromium and some vanadium-base alloys: A comparison with austenitic stainless steel. *J. Less Common Met.* **1969**, *19*, 39–51. [CrossRef]

18. Börm, H.; Schirra, M. Zeitstand- und kriechverhalten von Vanadin-Titan und Vanadin-Titan-Niob-legierungen. *Z Metallkde* **1968**, *59*, 715–723.

19. Börm, H.; Schirra, M. Untersuchungen über das zeitstand- und kreichverhalten binärer und ternärer vanadin-legierungen. *J. Less Common Met.* **1967**, *12*, 280–293.

20. Fukumoto, K.; Matsui, H. Precipitation behavior of vanadium alloys during creep deformation in a liquid sodium environment. *Mater. Jpn.* **2008**, *47*, 611. (In Japanese) [CrossRef]

21. Impagnatiello, A.; Shubeita, S.M.; Wady, P.T. Monolayer-thick TiO precipitation in V-4Cr-4Ti alloy induced by proton irradiation. *Scr. Mater.* **2017**, *130*, 174–177. [CrossRef]

22. Impagnatiello, A.; Toyama, T.; Jimenez-Melero, E. Ti-rich precipitate evolution in vanadium-based alloys during annealing above 400 °C. *J. Nucl. Mater.* **2017**, *485*, 122–128. [CrossRef]

23. Impagnatiello, A.; Hernandez-Maldonado, D.; Bertali, G. Atomically resolved chemical ordering at the nm-thick TiO precipi-tate/matrix interface in V-4Ti-4Cr alloy. *Scr. Mater.* **2017**, *126*, 50–54. [CrossRef]

24. Chung, H.M.; Loomis, B.A.; Smith, D.L. Creep properties of vanadium-base alloys. *J. Nucl. Mater.* **1994**, *212–215*, 772–777. [CrossRef]

25. Fukumoto, K.; Matsui, H.; Candra, Y.; Takahashi, K.; Sasanuma, H.; Nagata, S.; Takahiro, K. Radiation-induced precipitation in V–(Cr,Fe)–Ti alloys irradiated at low temperature with low dose during neutron or ion irradiation. *J. Nucl. Mater.* **2000**, *283–287*, 535–540. [CrossRef]

26. Fukumoto, K.; Iwasaki, M. A replica technique for extracting precipitates from neutron-irradiated or thermal-aged vanadium alloys for TEM analysis. *J. Nucl. Mater.* **2014**, *449*, 315–319. [CrossRef]

27. Watanabe, H.; Muroga, T.; Nagasaka, T. Effects of Irradiation Environment on V-4Cr-4Ti Alloys. *Plasma Fusion Res.* **2017**, *12*, 2405011. [CrossRef]

28. Rice, P.M.; Zinkle, S.J. Temperature dependence of the radiation damage microstructure in V–4Cr–4Ti neutron irradiated to low dose. *J. Nucl. Mater.* **1998**, *258–263*, 1414–1418. [CrossRef]

29. Seeger, A. *Proceedings of 2nd United Nations International Conference on the Peaceful Uses of Atomic Energy, Geneva*; United Nations: New York, NY, USA, 1958; Volume 6, p. 250.

30. Kiritani, M. Microstructure evolution during irradiation. *J. Nucl. Mater.* **1994**, *216*, 220–264. [CrossRef]

31. Kinoshita, C.; Fukumoto, K.; Nakai, K. Radiation-induced microstructural change in ceramic materials. *Ann. Chim. Fr.* **1991**, *16*, 379.

32. Fukumoto, K.; Kimura, A.; Matsui, H. Swelling behavior of V–Fe binary and V–Fe–Ti ternary alloys. *J. Nucl. Mater.* **1998**, *258–263*, 1431–1436. [CrossRef]